IEEE Access
Multidisciplinary ⋮ Rapid Review ⋮ Open Access Journal

Received September 28, 2020, accepted October 18, 2020, date of publication October 21, 2020, date of current version November 3, 2020.

Digital Object Identifier 10.1109/ACCESS.2020.3032793

An LCC-SP Compensated Inductive Power Transfer System and Design Considerations for Enhancing Misalignment Tolerance

JUNFENG YANG[1], (Member, IEEE), XIAODONG ZHANG[1], KAIJIAN ZHANG[2], XIAOYAN CUI[3], CHAOQUN JIAO[1], AND XU YANG[1], (Student Member, IEEE)

[1]School of Electrical Engineering, Beijing Jiaotong University, Beijing 100044, China
[2]School of Computer Science and Engineering, University of New South Wales, Sydney, NSW 2052, Australia
[3]School of Automation, Beijing University of Posts and Telecommunications, Beijing 100876, China

Corresponding author: Xiaodong Zhang (xdzhang@bjtu.edu.cn)

This work was supported in part by the Fundamental Research Funds for the Central Universities under Grant 2019YJS168.

ABSTRACT This paper proposes a novel LCC-SP compensation topology for inductive power transfer (IPT) system and its tuning methods to enhance misalignment tolerance. The impedance condition and the constant current output characteristic of the newly proposed topology are analyzed, followed by a detailed derivation of compensation parameters based on the discussion about resonant tank. The realization of zero voltage switching (ZVS) and reactive power demand are discussed by theoretical deduction and numerical simulation. Then, the parameters detuning method to enhance misalignment tolerance is presented and it is found that a stable output current is maintained over a wide misalignment. Compared to traditional compensation topologies, the newly proposed compensation topology provides the advantages of easy achievement of ZVS, high design freedom and high misalignment tolerance. Finally, the IPT prototype with the LCC-SP compensation network is built and tested. The experimental results match well with the calculations, validating the correctness of theoretical analysis.

INDEX TERMS Inductive power transfer, compensation topology, zero voltage switching, misalignment tolerance.

I. INTRODUCTION

Inductive power transfer (IPT) systems with advantages of isolation, convenience and safety features, have attracted considerable attention in last several years, such as high-power applications including batteries charging of electric vehicles (EVs) [1]–[3] and low-power applications including mobile devices [4] and implanted implants [5], [6]. A typical IPT system consists of several stages: a high frequency inverter (HFI), a magnetic couplers, compensation networks on both sides and a rectifier circuitry for dc charging. A dc-dc converter may be added for impedance matching or output adjustment.

High efficiency and steady power transfer is the first and uppermost objectives for all IPT power applications. There are many studies to solve these problems, such as novel compensation topologies and parameters optimization [7], [8], magnetic couplers design for larger coupling coefficient [9]–[11], control techniques for obtaining desired output characteristics [12] and so on. Among these fields, compensation topology is essential for its determination of resonant frequency, power factor, output characteristics to achieve higher system efficiency, power density, and reliability.

A number of IPT compensation networks in both primary and secondary sides have been developed and implemented to minimize the VA rating of the power supply. Four basic compensation topologies, namely, serial-serial (SS), serial-parallel (SP), parallel-serial (PS), and parallel-parallel (PP), are mainly researched in recent years [13]–[18]. Among these four topologies, SS compensation topology is applied most widely because the resonant frequency is independent of coupling coefficient [16]. Only two necessary compensation capacitors in SS topology, resulting in lower cost, smaller size, less power loss, and higher power density [17]. However, SS topology has two prominent deficiencies—low design

The associate editor coordinating the review of this manuscript and approving it for publication was Chi-Seng Lam.

freedom and high sensitivity to misalignment [18]. The first shortcoming reduces system flexibility from the constraint by loosely coupled transformer (LCT) parameters. High sensitivity to misalignment indicates that when relative position of two coupling coils changes, the performance of system deteriorates rapidly. Furthermore, large misalignment brings in infinite currents across primary capacitor and inductor, which would damage the power supply.

Therefore, some other high-order compensation topologies have been proposed recently. In [19], a novel S/CLC topology was proposed with the advantages of freedom from LCT, constant voltage output (CVO) and easy achievement of zero phase angle (ZPA). However, the voltage distortion of primary coil is serious, which is greatly affected by the load. The problem of current surge caused by misalignment still exists. It is necessary to apply higher order compensation for the primary side and additional protection circuit can be omitted. Based on symmetrical T-type compensation network, LCL topology was proposed in [20]–[23], where the compensation inductance was determined in terms of power balance between the inverter and the resonant tank. Although LCL compensation topology has the design freedom to realize load-independent constant output current (CCO) and input ZPA simultaneously, the compensation inductance should be equal to the self-inductance of coupling coil, which is usually quite large to transfer more power. This prominent problem leads to large power dissipation and relatively low system efficiency. Therefore, by employing additional capacitor in series to coils, partly reactive power compensated dispersedly, LCL evolve into LCC, which have contributed some practical topologies, such as S-LCC [24], LCC-S [25], LCC-P [26], double-sided LCC (DLCC) [27]–[29]. From the perspective of smoothing power transfer, an improved LCC type IPT system that features with distinct parameter design approach is proposed in [25]. To date, many researchers have studied DLCC compensation, and there are some methods to implement zero voltage switching (ZVS). With the tuning method presented in [27], the resonant frequency was irrelevant with coupling coefficient and load condition. Li *et al.* [29] applied DLCC compensation topology in dynamic electric vehicle (EV) charging and Li *et al.* [28] compared the characteristics of the SS and DLCC compensation topologies, implying outstanding advantages of not only improvement of high design freedom, but also achievement of desirable output current characteristics. However, the above DLCC parameter analysis are operated in the case of small resistance load or high coupling coefficient, in which case the rectifier works in continuous conduction mode (CCM), the current distortion is not serious and the ac load has little influence on the input impedance angle. Nevertheless, when the input voltage is low or the coupling coefficient is low, and the load is large, the rectifier current or voltage will appear discontinuous [29], [30]. The non-linear rectifier circuit introduces reactance component which increase diode loss. This problem has also been studied in some literatures, and the methods include frequency regulation [31], the addition of an adjustable inductor [29], or a third capacitor [32]. These methods are optimized for the second time after the parameter designs are completed, which increase the complexity of analysis.

Another unique feature of IPT systems is the high spatial freedom of coupling coils. Usually, the transmission stability of the system is highly dependent on the spatial magnetic coupling. Moreover, the system parameters and resonance frequency of compensation network are designed according to the coupling situation. The inevitable air-gap variation and misalignment of coils make the issue of enhancing tolerance to variation of coupling coefficient get more attention. In [33], the SP/S high-misalignment tolerant topology was elaborated, which combined the characteristics of SS and PS configurations. This topology makes rated power transfer with 25% misalignment but the range of coupling coefficient is not given. An S/SP type compensation topology is introduced in [34]. The method has the merit of coupling-insensitive gain at the intersection point with zero input phase angle of the input impedance, realizing robust reaction to coupling coefficient as well as load condition. In [35], the primary and secondary capacitance detuning categories is identified to have smooth power profile against varied coupling condition. The maximum power drop of SS compensated system is not more than 20% over 200% of coupling variation. However, when coupling condition varies quickly within wide range, the dynamic performance of the system is challenged and effective power transfer is likely to fail. For higher order compensation topology, Feng *et al.* [25] kept transmission power stable of the LCC-S compensated system by optimizing the parameters of compensation network at the selected coupling coefficient, simultaneously promising maximum transmission power and efficiency. A novel series-hybrid topology in [36] which the series inductors of the primary and pick-up LCL networks were integrated to improve the system performance under pad misalignment. The system utilized polarized magnetic couplers, resulting limit in the ability of directional anti-misalignment. The aforementioned literatures mainly focuses on maintaining voltage output, however, the stable output of IPT system is more desirably a current source in some applications, such as constant-current charging stage of EVs.

From the perspective of excellent CCO demand and smoothing the transmission power fluctuation, a novel LCC-SP compensation topology and the parameters optimization methods are proposed. T model of LCT and leakage compensation method are used in this paper's parameters design. The weak inductive input impedance angle makes ZVS realized easily, which can improve the efficiency of IPT system. Simultaneously, ZVS can be implemented for wide load and large coupling range. Furthermore, the proposed system does not suffer from the constraints of LCT parameters, since system output power can be readily altered by altering compensation parameters instead of replacing the LCT. This paper is organized as follows. Section II briefly introduces the problems of conventional DLCC compensated system.

To overcome these problems, the design method of newly proposed compensation topology and the CCO characteristic, together with the realization of ZVS are analyzed subsequently. The output current fluctuation under wide coupling coefficient is analyzed and the method to enhance misalignment tolerance is proposed in Section III. A practical example is designed and manufactured in Section IV to demonstrate the feasibility and effectiveness of proposed compensation topology. Finally, Section V concludes this paper.

II. TOPOLOGY DESIGN

A. PERFORMANCES OF CONVENTIONAL DLCC COMPENSATED SYSTEM

In many applications, such as batteries of electric vehicle and mobile devices, direct voltage or current outputs of IPT systems are demanded. Therefore, the rectifier circuit is needed to convert high frequency alternating component into direct component, and then supply dc power for actual load, or other dc-dc converters. For conventional analysis of DLCC compensation topology, the rectifier load is treated as a resistance load. However, the rectifier load is nonlinear and does not act simply as an equivalent resistor. The equivalent impedance of rectifier load is actually complex, containing resistive part and imaginary part, and the equivalent value is affected not only by its parameters, but also by the pre-stage impedance matching circuit [33], which cannot be easily simplified into linear impedance. Through the DLCC resonant compensation network, both real and reactive components of rectifier load are reflected to the inverter, which presents capacitive, as shown in Fig. 1 [37]. Here, u_{AB} and i_{AB} are output voltage and current of the inverter, while u_{ab} and i_{ab} are the input voltage and current of the rectifier diodes. The capacitive input phase angle of inverter introduces turn-off switching loss of the MOSFETS, representing a large part of the total power loss. To minimize the switching loss, it is better that

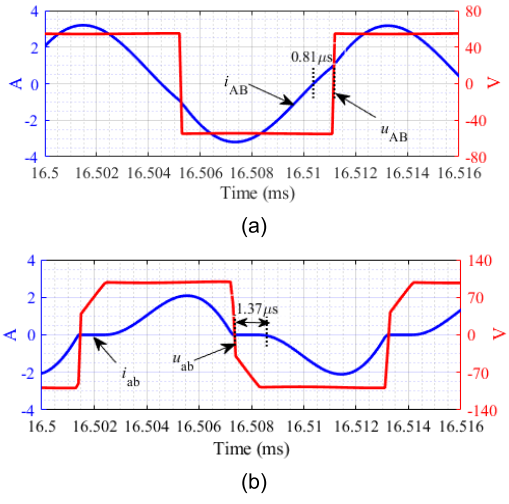

FIGURE 1. Simulation waveforms of DLCC compensation system. (a) Output voltage and current waveforms of inverter. (b) Input voltage and current waveforms of rectifier and dc current waveform of load.

switches operate at a ZVS condition, i.e. the inverter output current should lag behind output voltage.

Another disadvantage of the rectifier and associated regulating circuitry is distortions of current waveforms, resulting in discontinuous conduction mode (DCM) of rectifier. This deficiency is intuitively exhibited in Fig. 1(b) for an IPT system with 1 A terminal output. The diodes do not conduct all the time,which means almost one quarter of the time is not utilized and causes great waste of employed diodes. Moreover, a larger peak value of *i* ab leads to more power loss and higher current stress, driving down the system efficiency. Furthermore, precise theoretical analysis on the output current becomes more difficult due to discontinuity and distortion of the rectifier's input current. In light of the analysis in [37], the operation mode of DCM and CCM (continuous conduction mode) is related to the ratio of voltage over the parallel capacitor U_C to dc output voltage U_{DC}. When the ratio of U_{DC} to U_C is bigger than 0.7595, the input current of the full-wave diode rectifier (FDR) is discontinuous. It means that it is easier to enter DCM mode for light load (100 Ω in Fig. 1(b)).

B. PARAMETERS TUNING METHOD OF PROPOSED LCC-SP COMPENSATION TOPOLOGY

The proposed LCC-SP compensation network and corresponding power electronics circuit are shown in Fig. 2. U_d is original dc input voltage source. S_1-S_4 are four power MOSFETs in the primary side. D_1-D_4 are the secondary-side rectifier diodes. L_P and L_S are the self-inductances of the transmitting and receiving coils, respectively. L_{P1}, C_{P1} and C_{P2} are the primary-side compensation inductor and capacitors, forming the LCC compensation network. C_{S1} and C_{S2} are the secondary-side compensation components, forming the SP compensation network, where the S and P represents in series and in parallel with receiving coil. M is the mutual inductance between the two coils. L_f is filter inductor and C_f is filter capacitor. R_O is the practical resistive load. The parasitic resistances on the inductors and capacitors are neglected for simplicity of analysis.

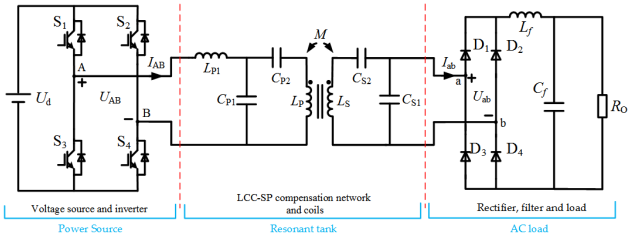

FIGURE 2. Circuit diagram of LCC-SP compensated IPT system.

Owing to the filtering function of compensation network, the fundamental harmonic approximation (FHA) is employed. In the following analysis, U_{AB}, U_{ab}, and I_{ab}, I_{ab}, are adopted to represent the first-order harmonics of the corresponding variables. When the duty cycle of the inverter is 50%, the relationship between input voltage U_{AB} of

resonant tank and the dc voltage U_d can be expressed as follow equation:

$$U_{AB} = \frac{2\sqrt{2}}{\pi} U_d. \tag{1}$$

After the output low-pass filter, the output current I_{RO} can be derived as

$$I_{RO} = \frac{\sqrt{2}\pi}{4} I_{ab}. \tag{2}$$

The rectifier load is nonlinear and contains high-order components, but the reactance part is not easy to express with a certain value. Generally, compared with the resistive part, the reactance component is small. For simplicity of analysis, the circuit of the diode rectifier, LC filter, and resistive load, is still replaced by its equivalent resistance R_E, which can be calculated by

$$R_E = \frac{\pi^2}{8} R_O. \tag{3}$$

At present, there are two kinds of compensation methods for different models of loosely coupled transformer in wireless charging system. One method adopts mutual inductance model, and the main idea is to compensate self-inductance. Another type of T model of LCT is to compensate leakage and mutual inductance, which is adopted here. Taking two mutual inductance coils as a whole and replacing LCT with its T-type model, the analytical circuit of Fig. 2 can be derived, as shown in Fig. 3. The apostrophe symbol " ′ " indicates the corresponding variables of the secondary side reflected to primary side.

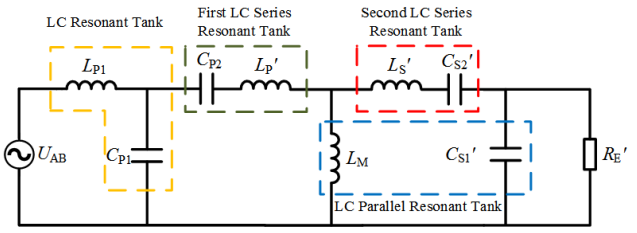

FIGURE 3. Analytical circuit of LCC/SP compensation topology.

For magnetic structures, the turn ratio of ideal transformer between the primary to secondary side is defined as

$$n = \sqrt{\frac{L_P}{L_S}}. \tag{4}$$

L_P' and L_S' in Fig. 3 are the leakage inductances of primary and secondary coils respectively while L_M stands for the primary converted mutual inductance. With $M = k\sqrt{L_P L_S}$, L_P', L_S' and L_M can be calculated by the following equations:

$$\begin{cases} L_P' = (1-k)L_P \\ L_S' = (1-k)n^2 L_S \\ L_M = nM, . \end{cases} \tag{5}$$

where k is the coupling coefficient between the primary and secondary coils. C_{S1}', C_{S2}' and R_E' are the primary-referred values of C_{S1}, C_{S2} and R_E, respectively. According to the T-type model of the LCT, C_{S1}', C_{S2}' and R_E' can be derived as

$$\begin{cases} C_{S1}' = C_{S1}/n^2 \\ C_{S2}' = C_{S2}/n^2 \\ R_E' = n^2 R_E. \end{cases} \tag{6}$$

In this paper, C_{P2} is designed to resonate with L_P' in series and C_{S2}' and L_S' make up a series resonant tank. L_M and C_{S1}' form a parallel resonant tank. All resonant angular frequencies equal ω_S, the system operating angular frequency. Then the following equations can be yielded:

$$\omega_S^2 = \frac{1}{L_P' C_{P2}} = \frac{1}{L_S' C_{S2}'} = \frac{1}{L_M C_{S1}'}. \tag{7}$$

According to circuit theories, LC series resonance is equivalent to short circuit and parallel resonance is equivalent to open circuit. When all resonances satisfy (7), the equivalent circuit can be simplified as the voltage source U_{AB} transfers energy to the equivalent load R_E' through the series inductance L_{P1} and the parallel capacitance C_{P1}. When L_{P1} resonates with C_{P1}, i.e. (8) is satisfied, according to constant voltage input to constant current output characteristic of an LC resonant tank, the current I_{ab}' over R_E' can be deduced as shown in (9)

$$\omega_S^2 = \frac{1}{L_{P1} C_{P1}}, \tag{8}$$

$$I_{ab}' = -jU_{AB}\sqrt{\frac{C_{P1}}{L_{P1}}} = -j\frac{U_{AB}}{\omega L_{P1}}. \tag{9}$$

On the basis of (9), if U_{AB} is constant, the output current I_{ab}' of LC resonant tank will be also constant, having nothing to do with the load. In terms of the relationship between primary-referred value of resistance R_E' and the actual load R_E, the current I_{ab} through R_E and the output current I_{RO} through R_O can be yielded

$$I_{ab} = nI_{ab}' = -j\frac{nU_{AB}}{\omega L_{P1}}, \tag{10}$$

$$I_{RO} = \frac{nU_d}{\omega_S L_{P1}}. \tag{11}$$

The entire resonant tank composed of LCC-SP compensation network shows a constant current output characteristic.

Equation (11) also indicates that LCC-SP compensated IPT system is free from the LCT constraints imposed as n, on account of introduced L_{P1}. I_{RO} can be readily altered by changing L_{P1}. The increasing degree of design freedom is very helpful in the scenarios with strict coil size limitations. The average power consumed by R_O can be subsequently obtained as

$$P_{RO} = \frac{U_d^2 L_P}{(\omega_S L_{P1})^2 L_S} R_O. \tag{12}$$

C. ZVS AND CCM REALIZATION

To reduce the switching loss and improve system efficiency, we prefer to achieve zero voltage switching (ZVS) condition. For a full-bridge converter, this means the resonant current slightly lags the resonant voltage which forms the ZVS operation condition for all MOSFETs. For analytic simplification, an input impedance Z_{in} of inverter is defined.

Under perfect resonant conditions, which mean that L_P', L_S', and L_M resonate with C_{P2}, C_{S2}' and C_{S1}', respectively, the input impedance Z_{in} seen from Fig. 3 can be deduced as

$$Z_{in} = Z_{LP1} + \frac{Z_{CP1}Z'_{RE}}{Z_{CP1} + Z'_{RE}}, \tag{13}$$

where Z_{RE}' is the referred equivalent impedance parallel to the compensation capacitor C_{P1}. Substituting (3) and (6) into (13), Z_{in} can be depicted as

$$Z_{in} = \frac{8(\omega_S L_{P1})^2}{64(\omega_S L_{P1})^2 + \pi^4 n^4 R_O^2}(\pi^2 n^2 R_O + j8\omega_S L_{P1}). \tag{14}$$

The input impedance angle θ can be obtained as

$$\theta = \frac{180^\circ}{\pi} \arctan \frac{8\omega L_{P1}}{\pi^2 n^2 R_O}. \tag{15}$$

It can be seen from (15) that the input impedance Z_{in} is always inductive and the inductance L_{P1} and coil ratio n exert an influence on the input impedance angle θ. As a comparison, the input impedance of inverter for a 100 Ω load resistance is shown in Fig. 4. The values of compensation components L_{P1}, C_{P1}, C_{S1} and two coils L_{P}, L_{S} are same as previous mentioned DLCC compensation topology. In terms of Fig. 4 (a), the output current slightly lags behind output voltage, only 10.1°. The efficiency of IPT technology is improved with near zero input reactive power. The input impedance angle keeps positive with respect to different resistance and tends to be small and stable with larger load.

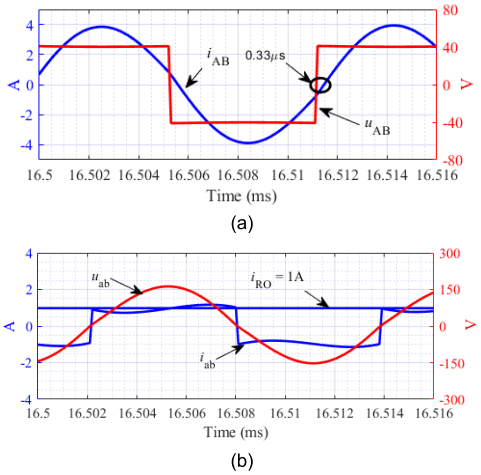

FIGURE 4. Simulation waveforms of proposed LCC-SP compensation system. (a) Output voltage and current waveforms of inverter. (b) Input voltage and current waveforms of rectifier and dc current waveform of load.

After the LCC-SP compensation network, the power transmission converts to a constant source, and U_{ab} over the rectifier works between CCM and DCM. The method in [37] is still available, but the criteria of work modes becomes the ratio of load current I_{RO} and receiving coil current I_{S}, which can be given as

$$\frac{I_{RO}}{I_S} = \frac{|Z_{SC1}|}{|Z_{SC1} + Z_{RE}|}. \tag{16}$$

When the ratio is smaller than 0.7595, the input voltage is continuous. For light load, it is easier to work under continuous conduction mode. Fig. 4 (b) presents the input voltage and current waveforms of rectifier. The resistance of load is 100 Ω and the ratio can be calculated as 0.510, much smaller than the critical value 0.7595. From Fig. 4 (b), the input waveform of u_{ab} is near-sinusoidal, holding continuous over time. The drawback of a conventional DLCC system, discontinuous input current of rectifier dissolves.

III. ENHANCEMENT OF MISALIGNMENT TOLERANCE

In this section, the general output current with respect to varied coupling coefficient is elaborated and studied firstly. The mutual inductance model is applied to calculate electrical quantities in the target system. By comparing different detuned performances, the suitable compensation is identified to build the high misalignment tolerant IPT system.

A. OUTPUT CURRENT UNDER MISALIGNED SITUATION

The core component of an IPT system is magnetic couplers with the conventional transformer replaced by a loosely coupled transformer. The relative position between the primary and secondary windings is normally changeable, introducing variations in the values of inductances and coupling coefficient of the transformer [12]. Therefore, an IPT system should tolerate not only a large variation of load, but also a wide range of coupling coefficient.

The LCC-SP compensation system shows an excellent CCO characteristic and has nothing to do with the coupling coefficient under perfect resonant condition. However, the output current no longer conforms to (11) due to the misalignment. In the following section, the form of impedance is employed to represent the values of compensate components. According to the design methods of compensation network in the Section II, adopt k_0 to represent the coupling coefficient under normal operation, we can get the relations between C_{S1}, C_{S2} and L_{S} as

$$k_0 Z_{LS} + Z_{SC1} = 0, \tag{17}$$

$$(1 - k_0) Z_{LS} + Z_{SC2} = 0. \tag{18}$$

Then the secondary impedance Z_{S} and reflected impedance Z_{r} to the primary side can be obtained

$$Z_S = \frac{(k_0 Z_{LS})^2}{k_0 Z_{LS} - Z_{RE}}, \tag{19}$$

$$Z_r = \left(\frac{k}{k_0}\right)^2 (n^2 Z_{RE} - k_0 Z_{LP}). \tag{20}$$

Z_{CP2} and Z_{LP} designed in resonance condition have the following relation

$$(1-k_0)Z_{LP}+Z_{CP2}=0 \tag{21}$$

The total series impedance of C_{P2}, L_P and Z_r is given as

$$Z_{Tr}=\left(k_0-\frac{k^2}{k_0}\right)Z_{LP}+\left(\frac{nk}{k_0}\right)^2 Z_{RE}. \tag{22}$$

The input impedance of the inverter can be deduced as

$$Z_{in}=Z_{LP1}+\frac{Z_{CP1}Z_{Tr}}{Z_{CP1}+Z_{Tr}}. \tag{23}$$

Based on Kirchhoff's law, the currents through L_{P1}, L_P and equivalent load R_E can be yielded

$$\begin{cases} I_{LP1}=\dfrac{U_{AB}}{Z_{in}} \\ I_{LP}=I_{LP1}\dfrac{Z_{CP1}}{Z_{CP1}+Z_{CP2}+Z_{LP}+Z_r} \\ I_{LS}=\dfrac{j\omega MI_{LP}}{Z_S} \\ I_{ab}=I_{LS}\dfrac{Z_{CS1}}{Z_{CS1}+Z_{RE}}. \end{cases} \tag{24}$$

Therefore, for the load before the rectification, the following equation between the load current I_{ab} and the inverter output voltage U_{AB} can be calculated as

$$I_{ab}=-j\frac{nk}{k_0}\frac{U_{AB}}{Z_{LP1}}. \tag{25}$$

When the positions of the two coils make k equal to k_0, the output current I_{ab} is the same as that of (10). The output current increases linearly when k increases from 0 to 1, which means great output current fluctuation. The misalignment tolerance of unmodified LCC-SP compensation topology is relatively low and not practical.

B. MODIFIED PARAMETERS TUNING METHOD

Some previous works have pointed out that parameters optimization in topology are simple but efficacious to minimize the power fluctuation [32], [33]. The resonant L_{P1} and C_{P1} determine the output current, which is suitable for misalignment study. The fully tuned configuration of the coupling transformer is fabricated, i.e. C_{P2} and the reflected capacitance of C_{S1} and C_{S2} should be compensate L_P', L_M, L_S' with well aligned k_0. Since magnetic couplers is main components of power transmission, L_P and L_S are the basic premise of parameters design. Thus taking the impedance of L_P as reference, the detuned impedance factors of L_{P1} and C_{P1} are defined as follows:

$$\alpha=\frac{|Z_{LP}|}{|Z_{CP1}|}, \tag{26}$$

$$\beta=\frac{|Z_{LP1}|}{|Z_{LP}|}. \tag{27}$$

Replacing the L_{P1} and C_{P1} with α and β, the current across the transmitter coil can be updated as

$$I_{LP}=\frac{U_{AB}}{((1-\alpha\beta)\left(\frac{k^2}{k_0}+k_0\right)+\beta)Z_{LP}+(1-\alpha\beta)\left(\frac{nk}{k_0}\right)^2 Z_{RE}}. \tag{28}$$

Substituting (28) into (24), the output current I_{ab} is given as

$$\begin{aligned} I_{ab}&=\frac{U_{AB}}{\left(-(1-\alpha\beta)nk+\frac{((1-\alpha\beta)k_0+\beta)nk_0}{k}\right)Z_{LS}+\frac{(1-\alpha\beta)n}{k_0}kZ_{RE}} \\ &=\frac{U_{AB}}{X_{eq}+R_{eq}}. \end{aligned} \tag{29}$$

Consequently, the entire compensation network can be equivalent to a series impedance composed of the reactance X_{eq} and the resistance R_{eq}. Let

$$\begin{cases} A=-(1-\alpha\beta)n \\ B=((1-\alpha\beta)k_0+\beta)nk_0 \\ D=\dfrac{(1-\alpha\beta)n\,|Z_{RE}|}{k_0\,|Z_{LS}|}. \end{cases} \tag{30}$$

X_{eq} and R_{eq} can be rearranged as follows by replacing with A, B and D

$$\begin{cases} X_{eq}=\left(Ak+\dfrac{B}{k}\right)Z_{LS} \\ R_{eq}=Dk\,|Z_{LS}|. \end{cases} \tag{31}$$

Considering the terminal dc current after rectifying and filtering, the amplitude current needs to be concerned, which is discussed as

$$I_{\mathrm{Amp}}(\alpha,\beta,k)=\frac{\sqrt{2}\pi}{4}|I_{ab}|=\frac{|U_d|}{|X_{eq}+R_{eq}|}. \tag{32}$$

The derivative of $I_{\mathrm{Amp}}(\alpha,\beta,k)$ with respect to k can then be calculated

$$\frac{\partial I_{\mathrm{Amp}}}{\partial k}=-\frac{|U_{ab}|}{|Z_{LS}|}(\lambda^2+\kappa^2)^{-\frac{3}{2}}\left((A^2+D^2)k-\frac{B^2}{k^3}\right). \tag{33}$$

where $\lambda=Ak+B/k$, $\kappa=Ck$. Equation (33) indicates that the maximized I_{Amp} can be calculated by setting the derivative of $I_{\mathrm{Amp}}(\alpha,\beta,k)$. Using $Q_S=|Z_{LS}|/Z_{RE}$ for the secondary quality factor and solving $\partial I_{\mathrm{Amp}}/\partial k=0$, the extreme point can be obtain as

$$k_{opt}=q\sqrt{\left|k_0+\frac{\beta}{1-\alpha\beta}\right|}, \tag{34}$$

where

$$q=k_0\frac{1}{\sqrt[4]{k_0^2+\left(1/Q_S\right)^2}}. \tag{35}$$

The extreme point k_{opt} is determined by the detuned L_{P1} and C_{P1} and has an impact on its corresponding maximum current. To ensure a smooth current profile around nominal coupling coefficient, the point k_{opt} is set to equal k_0 and the

maximum current is set to nominal output current I_{nom}. Thus, for the same rated load and align situation, the currents of load are the same with tuned and detuned parameters. Taking k_0 coupling as the center, extend the coupling coefficient range of constant current in both directions. The minimum coupling coefficient is denoted as $k_{\min}$ and the maximum one is denoted as $k_{\max}$. The current fluctuations at the boundary coupling ($k_{\min}$, $k_{\max}$) are set to the same. The conditions for satisfying the stable power transmission are as follows:

$$k_{opt} = k_0, \tag{36.1}$$

$$I_{Amp}(k_{opt}) = I_{nom}, \tag{36.2}$$

$$I_{Amp}(k_{\min}) = I_{Amp}(k_{\max}). \tag{36.3}$$

Depending on the implement of (36), the designed parameters have clear and quantitative anti-misalignment capability. For instance, assuming that the demand current I_{Amp} is 1 A and the nominal coupling coefficient k_0 is selected as 0.3. Apparently, the load, represented as Q_{S}, reflects the impact of k_{opt} variation on output characteristics. To investigate the performance of different loads, the R_{O} is fixed as 50 Ω, 100 Ω and 150 Ω, corresponding Q_{S} is 1.56, 0.78 and 0.52, respectively. The expressions of k_{opt} and I_{Amp} are complicate and the numerical analysis tool MATLAB is used. Fig. 5 (a) exhibits the profiles of factor solutions when k_{opt} equals k_0. For each Q_{S}, the distributions of detuned factors α and β are on two sides of the resonance line ($\alpha^*\beta = 1$). The detuned factors of L_{P1} is reversely proportional to the detuned factors of C_{P1}. Meanwhile, the curve with smaller Q_{S} is closer to the resonance line. The effects of different Q_{S} on the maximum output current I_{Amp} are shown in Fig. 5 (b). In terms of Fig. 5 (b), an intersection point M_0 (4.163, 0.240) comes about through three solution lines. In essence, it is the tuned point at which L_{P1} resonate with C_{P1}. In order to make the maximum output current equal to the rated output current, it is necessary to bring about larger α and smaller β than resonance point.

Therefore, at the nominal coupling coefficient k_0, the solutions of the maximum output current $I_{\text{Amp}}(k_{\text{opt}})$, which equal to the rated value I_{nom} can be obtained, as shown in the Fig. 5 (c). Denoted by M_{i} and N_{i} ($i = 1, 2, 3$), each analytical solutions are far away from resonance point and distributed on both sides of the resonance line. Among them, M_1, M_2 and M_3 are located at (5.926, 0.203), (5.932, 0.188) and (5.926, 0.182), respectively, while N_1, N_2 and N_3 are positioned at (5.305, 0.129), (5.716, 0.149) and (5.795, 0.156). The products of α and β in M_{i} are less than 1, nevertheless the product of α and β in N_{i} is greater than 1. The different effects of M_{i} and N_{i} on the system are reflected in the input impedance. As shown in Fig. 6, the input impedance of inverter with M_{i} is inductive around nominal coupling coefficient, desirable for the inverter to have ZVS. However, the currents across MOSFETs with N_{i} lead the voltages, which brings great switch losses and is not suitable for practical application.

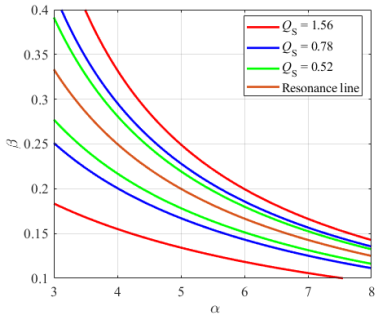

(a)

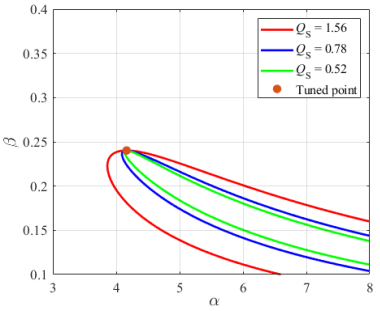

(b)

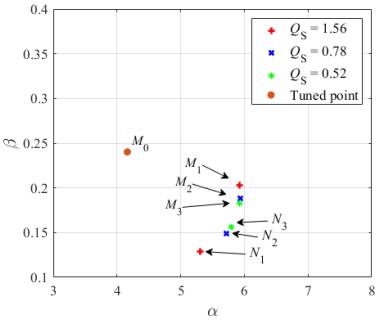

(c)

FIGURE 5. Curves of solution to satisfy stable output current. (a) k_{opt} satisfying (36.1). (b) I_{Amp} satisfying (36.2). (c) Solution points satisfying (a) and (b).

The output current characteristics of M_{i} against various coupling coefficient are given in Fig. 7. It is assumed that the stable current needs to fluctuate less than 10%, i.e. the output current cannot be less than 0.9A. By 36.3, $k_{\min}$ and $k_{\max}$ are obtained. In order to distinguish the misalignment characteristics, regions close to $k_{\min}$ and $k_{\max}$ are zoomed in. For three sets of optimized parameters, the currents is collectively kept within a wide flat region. When Q_{S} equals 1.56, the minimum $k_{\min} = 0.201$ and the maximum $k_{\max} = 0.446$ are obtained, nearly 112% coupling variation. The current fluctuation tendencies of $Q_{\text{S}} = 0.78$ and 0.52 are

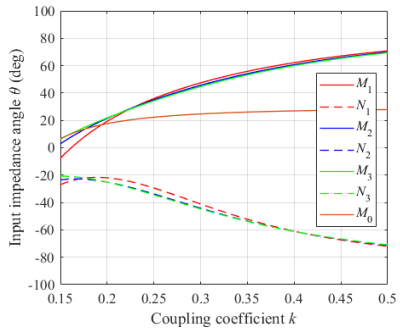

FIGURE 6. Input impedance phase angle of different combinations of α and β against varied coupling coefficient k.

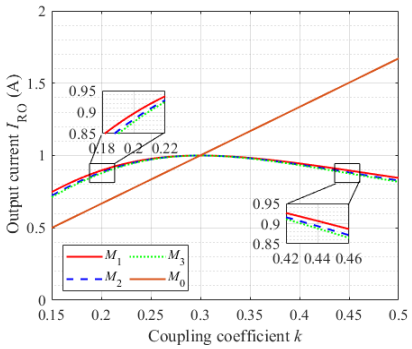

FIGURE 7. Output current fluctuations against varied coupling coefficient for three sets of M_{i} ($i = 0, 1, 2, 3$).

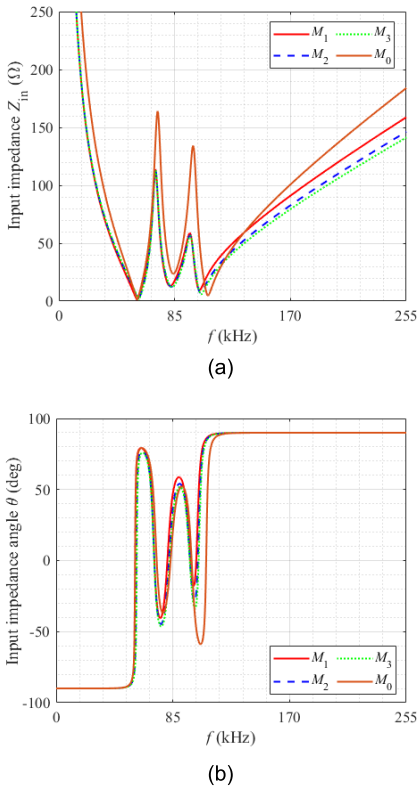

FIGURE 8. Curves of input impedance versus working frequency with $M_{\mathrm{i}}(i = 0, 1, 2, 3)$. (a) Amplitude characteristic. (b) Phase characteristic.

same as 1.56, the coupling coefficient range of maintaining transmission power are (0.207, 0.435) and (0.209, 0.430), respectively. When the small Q_{S} is applied to the system, the coupling range with stable current is narrowed down slightly. The feasible coupling coefficient variation in the narrowest range is still more than 105% (from 0.209 to 0.430). Compared with the output current linearly increased under the tuned parameter M_0, the anti-misalignment performance has been greatly improved. In addition, it can be seen from Fig. 5 (c) that the distributions of M_{i} are relatively concentrated, which indicates that M_{i} has not only the characteristics of misalignment tolerance, but also the ability to maintain stable output under a wide range of loads. This can also be verified from Fig. 7, where the load ranges from 50 Ω to 150 Ω but the fluctuation curves are very close. Consequently, it can reveal that the optimized methods of detuned L_{P1} and C_{P1} provide admirable robust reaction to the variation of both coupling coefficient and loads.

For different sets of M_i ($i = 0, 1, 2, 3$), the input impedance profiles versus working frequency are exhibited in Fig. 8. Fig. 8 (a) indicates the trends of the curves are similar, where the input impedance of high-order harmonic is much larger than that of the fundamental component (85 kHz), resulting in small harmonics in the current flowing through L_{P1}, contributing to near-sinusoidal output current of the inverter. Fig. 8 (b) shows that the input impedance angles are inductive at operation frequency in tuned and modified situation. The leading phase angle of the detuned parameters is larger than that of the resonance parameters, equaling 14° with M_0 and 42° with M_1, respectively. The input impedance angles of second and higher harmonics equal 90°, only reactive power can be produced. Fig. 8 suggests that the excellent high-order harmonic suppression capacity of LCC-SP system is achieved to reduce power loss and improve system efficiency.

IV. EXPERIMENTAL VERIFICATION

The experimental setup for the integrated LCC-SP compensation IPT system is built and shown in Fig. 9. A high power dc supply is used to transfer energy to high frequency inverter and an electronic load is used to replace the battery load after rectifier. TMS320F28335 DSP, implemented as controller, is responsible for sending PWM signals to the inverter. The specifications of the studied prototype are tabulated in Table 1. The available resistance and current of load are 50 Ω and 1 A, leading to 50 W rating wireless power transfer system. The dc bus voltage is 42 V, slightly greater than the theoretical value for the power loss on diverse components.

The experimental output dc voltage and current with no misalignment at two different loads stage are shown in Fig. 10. In the beginning, the load is at 100 Ω. U_{RO} and I_{RO} are 98.35 V and 0.984 A. When the resistance suddenly drops to 50 Ω, U_{RO} decreases from 98.35 to 52.68 V, nearly half of the normal value. After an instant surge, I_{RO} drops

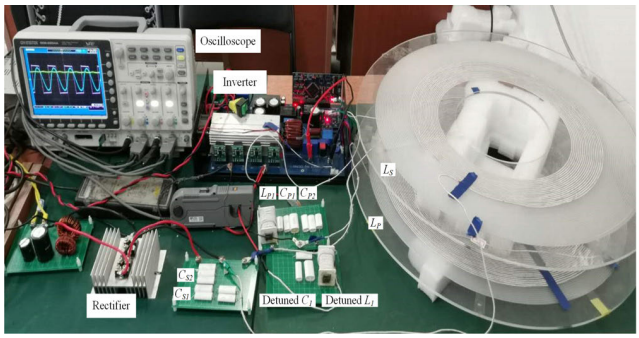

FIGURE 9. Experimental setup for LCC-SP system.

TABLE 1. Some critical parameters adopted in the simulation.

Symbol	Parameters	Value
U_d	Input dc voltage	42 V
f	Switching frequency	85 kHz
k	Coupling coefficient	0.15-0.5
L_{P1}	Primary compensation inductance	126.1 μH
L_P	Transmitting coil inductance	540.2 μH
L_S	Receiving coil inductance	180.1 μH
C_{P1}	Primary parallel compensation capacitor	27.61 nF
C_{P2}	Primary series compensation capacitor	9.25 nF
C_{S1}	Secondary parallel compensation capacitor	65.12 nF
C_{S2}	Secondary series compensation capacitor	27.49 nF
α	Impedance deviation of L_{P1}	5.907
β	Impedance deviation of C_{P1}	0.206

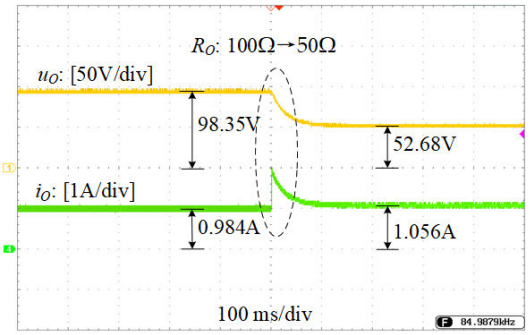

FIGURE 10. CCO characteristic of proposed LCC-SP compensation topology.

to 1.056 A, which is only 7.32% larger than the previous value, showing excellent CCO characteristic. For resistances equal to 100 Ω and 50 Ω, the output waveforms of HFI and the input waveforms of diode rectifier are shown in Fig. 11. Under 100 Ω resistance load, the current lag phase angle is close to zero, as slightly inductive. When the resistance alters to 50 Ω, the angle that the current leads the voltage is about 11°, indicating the realization of ZVS and reduction of switching loss. The input voltage of rectifier keeps continuous always and mainly discrepancy is the amplitude of the near-sinusoidal waveform. Experimental results coincide well with the theoretical analysis.

Fig. 12 shows the output current and efficiency curves of IPT system with varied load from 30 Ω to 100 Ω. The efficiency is the entire system efficiency from the dc input power to the electronic load. The output current decreases linearly with the resistance, from 1.09A to 0.96A, and

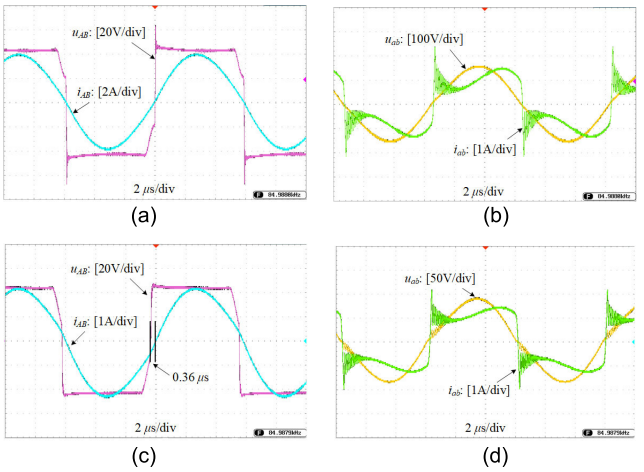

FIGURE 11. Experimental waveforms of system. (a) Output waveforms of inverter when $R_O = 100$ Ω. (b) Input waveforms of rectifier when $R_O = 100$ Ω. (c) Output waveforms of inverter when $R_O = 50$ Ω. (d) Input waveforms of rectifier when $R_O = 50$ Ω.

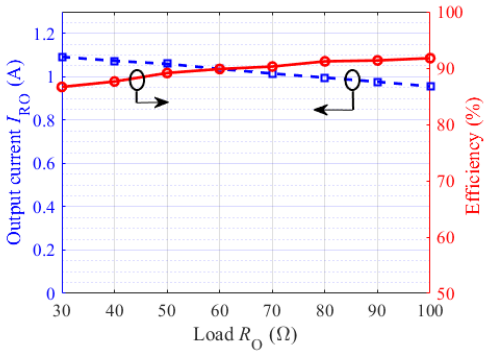

FIGURE 12. Output current and transmission efficiency versus load R_O.

the fluctuation maintains within 10% of the rated output current. The efficiency of the system increases from 86.7% to 91.8%. The power loss of the IPT system mainly consists of the switching loss of inverter, stray loss caused by parasitic resistance in compensation network, transmitting coil and receiving coil. Under resonant state, the high efficiency is maintained.

Considering conditions of misalignment, the detuned $C_{P1} = 38.33$ nF and $L_{P1} = 111.2$ μH are adopted, where α is 5.907 and β is 0.206. This calculation factors are based on the resistor of 50 Ω. The experimental waveforms are provided in Fig. 13, the ZVS condition is maintained regardless of coupling coefficient and the input impedance changes to capacitive only with very small coupling coefficient. Fig. 14 exhibits the profile of output current i_{RO} with respect to coupling coefficient of the LCT. In comparison, the system with tuned parameters is also fabricated. It can be seen that the current decreases rapidly with decreasing coupling coefficient and the current at coupling of 0.2 drops below 55% of current at coupling of 0.5, whose fluctuation is much larger than the modified detuned one. From Fig. 14, with detuned parameters, the output current fluctuations is less than 10 % when the coupling coefficient changes about 250% (from 0.2 to 0.5).

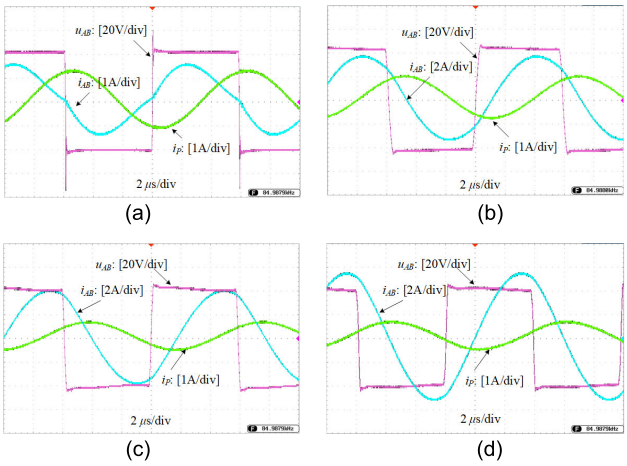

FIGURE 13. Experimental waveforms of system Output waveforms of inverter and current of transmitting coil with detuned LCC-SP compensation. (a) $k = 0.15$. (b) $k = 0.3$. (c) $k = 0.4$. (d) $k = 0.5$.

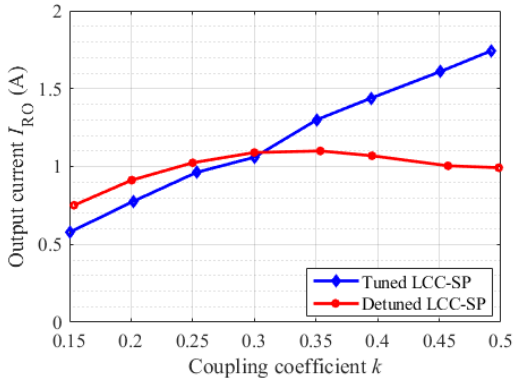

FIGURE 14. Experimental results of output current versus coupling coefficient k.

The maximum current is 1.09 A when the coupling coefficient is around 0.3, a little higher than 1.05 A in tuned condition. The deviation of the results come from the effect of parameter shift and stray loss. The tendencies of results show good agreement with theoretical analysis. The comparison results demonstrate an extremely good misalignment tolerance capability with detuned parameters.

Since the ZVS state can be naturally realized under tuned and detuned LCC-SP compensation topology, high efficiency of the system can be achieved. As shown in Fig. 15, when k is equal to 0.3, the efficiency under tuned parameters is 88.35%, the efficiency after detuning is 89.82%, and the efficiency fluctuation under two working conditions is only 1.47%. According to Fig. 14, the currents under two working conditions are 1.05A and 1.09A, and the current fluctuation is 3.81%. Both cases work in ZVS state, and the ratio of the loss to the total power is smaller when the current is high, so the efficiency increases slightly. When the coupling coefficient decreases, the inductance of the input impedance decrease, while there is no increase in reactive power. Since the output current is maintained and the inductance is weakened,

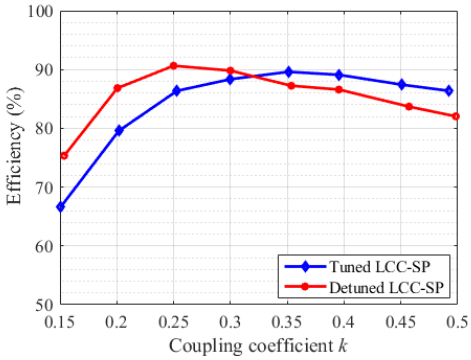

FIGURE 15. Transmission efficiency versus coupling coefficient k.

the efficiency will first have a growth trend. Then, the output current will decrease and the efficiency will begin to decline. However, under the tuned parameters, the output current drops rapidly with lessen coupling coefficient and the transmission capacity of the system decays. The system loss takes a greater part, which leads to a lower efficiency than detuned condition. In the detuned LCC-SP system, a high dc–dc efficiency over 80% is maintained in the range of k from 0.2 to 0.5. When the coupling strengthens more than 0.3, more reactive power is needed to transfer same quantity of real power. As a result, the efficiency is degraded worse than tuned system.

V. CONCLUSION

A novel compensation topology for IPT system, namely LCC-SP, is proposed in this paper. The reformed topology offers excellent CCO characteristic, which is verified by experiment. Analysis and experiment results suggest that the inherent ZVS can always be achieved, resulting in drastically reduced switching loss and remarkably simplified thermal design. Moreover, the LCC-SP system provides another degree of design freedom and disburdens the constraints imposed by the LCT parameters. Compared to DLCC compensation topology, proposed topology presents much better high-order harmonic suppression capability. The issue of discontinuous diode current dissolves because the input voltage of the rectifier diode is near-sinusoidal without serious distortion.

The improvement of misalignment tolerance is also studied. For different load, the analytical solutions of the optimal resonance parameters offer the strong anti-misalignment capability. By setting the maximum current at k_0, the output current is kept constant and high efficiency over 80% is maintained in the range of k from 0.2 to 0.5. Experimental results agree well with theoretical analysis, demonstrating the validity of the optimization method.

REFERENCES

[1] D. Patil, M. K. McDonough, J. M. Miller, B. Fahimi, and P. T. Balsara, "Wireless power transfer for vehicular applications: Overview and challenges," *IEEE Trans. Transport. Electrific.*, vol. 4, no. 1, pp. 3–37, Mar. 2018.

[2] G. Buja, M. Bertoluzzo, and K. N. Mude, "Design and experimentation of WPT charger for electric city car," *IEEE Trans. Ind. Electron.*, vol. 62, no. 12, pp. 7436–7447, Dec. 2015.

[3] R. Tavakoli and Z. Pantic, "Analysis, design, and demonstration of a 25-kW dynamic wireless charging system for roadway electric vehicles," *IEEE J. Emerg. Sel. Topics Power Electron.*, vol. 6, no. 3, pp. 1378–1393, Sep. 2018.

[4] H. H. Lee, S. H. Kang, and C. W. Jung, "MR-WPT with reconfigurable resonator and ground for laptop application," *IEEE Microw. Wireless Compon. Lett.*, vol. 28, no. 3, pp. 269–271, Mar. 2018.

[5] A. N. Abdulfattah, C. C. Tsimenidis, B. Z. Al-Jewad, and A. Yakovlev, "Performance analysis of MICS-based RF wireless power transfer system for implantable medical devices," *IEEE Access*, vol. 7, pp. 11775–11784, 2019.

[6] P. Chen, H. Yang, R. Luo, and B. Zhao, "A tissue-channel transcutaneous power transfer technique for implantable devices," *IEEE Trans. Power Electron.*, vol. 33, no. 11, pp. 9753–9761, Nov. 2018.

[7] G. de Freitas Lima and R. B. Godoy, "Modeling and prototype of a dynamic wireless charging system using LSPS compensation topology," in *Proc. Brazilian Power Electron. Conf. (COBEP)*, Juiz de Fora, Brazil, Nov. 2017, pp. 1–6.

[8] X. Qu, Y. Jing, H. Han, S.-C. Wong, and C. K. Tse, "Higher order compensation for Inductive-Power-Transfer converters with constant-voltage or constant-current output combating transformer parameter constraints," *IEEE Trans. Power Electron.*, vol. 32, no. 1, pp. 394–405, Jan. 2017.

[9] L. Zhao, S. Ruddell, D. J. Thrimawithana, U. K. Madawala, and P. A. Hu, "A hybrid wireless charging system with DDQ pads for dynamic charging of EVs," in *Proc. IEEE PELS Workshop Emerg. Technol., Wireless Power Transf. (WoW)*, Chongqing, China, May 2017, pp. 1–6.

[10] S. Bandyopadhyay, P. Venugopal, J. Dong, and P. Bauer, "Comparison of magnetic couplers for IPT-based EV charging using multi-objective optimization," *IEEE Trans. Veh. Technol.*, vol. 68, no. 6, pp. 5416–5429, Jun. 2019.

[11] F. Lu, H. Zhang, H. Hofmann, W. Su, and C. C. Mi, "A dual-coupled LCC-compensated IPT system with a compact magnetic coupler," *IEEE Trans. Power Electron.*, vol. 33, no. 7, pp. 6391–6402, Jul. 2018.

[12] M. Kim, D.-M. Joo, and B. K. Lee, "Design and control of inductive power transfer system for electric vehicles considering wide variation of output voltage and coupling coefficient," *IEEE Trans. Power Electron.*, vol. 34, no. 2, pp. 1197–1208, Feb. 2019.

[13] W. Zhang and C. C. Mi, "Compensation topologies of high-power wireless power transfer systems," *IEEE Trans. Veh. Technol.*, vol. 65, no. 6, pp. 4768–4778, Jun. 2016.

[14] X. Qu, W. Zhang, S.-C. Wong, and C. K. Tse, "Design of a current-source-output inductive power transfer LED lighting system," *IEEE J. Emerg. Sel. Topics Power Electron.*, vol. 3, no. 1, pp. 306–314, Mar. 2015.

[15] W. Zhou and H. Ma, "Design considerations of compensation topologies in ICPT system," in *Proc. IEEE Conf. Appl. Power Electron.*, Anaheim, CA, USA, Feb. 2007, pp. 985–990.

[16] C.-S. Wang, G. A. Covic, and O. H. Stielau, "Power transfer capability and bifurcation phenomena of loosely coupled inductive power transfer systems," *IEEE Trans. Ind. Electron.*, vol. 51, no. 1, pp. 148–157, Feb. 2004.

[17] Y. H. Sohn, B. H. Choi, E. S. Lee, G. C. Lim, G.-H. Cho, and C. T. Rim, "General unified analyses of two-capacitor inductive power transfer systems: Equivalence of current-source SS and SP compensations," *IEEE Trans. Power Electron.*, vol. 30, no. 11, pp. 6030–6045, Nov. 2015.

[18] C.-S. Wang, O. H. Stielau, and G. A. Covic, "Design considerations for a contactless electric vehicle battery charger," *IEEE Trans. Ind. Electron.*, vol. 52, no. 5, pp. 1308–1314, Oct. 2005.

[19] Y. Wang, Y. Yao, X. Liu, and D. Xu, "S/CLC compensation topology analysis and circular coil design for wireless power transfer," *IEEE Trans. Transport. Electrific.*, vol. 3, no. 2, pp. 496–507, Jun. 2017.

[20] X. Qu, H. Chu, Z. Huang, S.-C. Wong, C. K. Tse, C. C. Mi, and X. Chen, "Wide design range of constant output current using double-sided LC compensation circuits for inductive-power-transfer applications," *IEEE Trans. Power Electron.*, vol. 34, no. 3, pp. 2364–2374, Mar. 2019.

[21] Q. Zhu, L. Wang, Y. Guo, C. Liao, and F. Li, "Applying LCC compensation network to dynamic wireless EV charging system," *IEEE Trans. Ind. Electron.*, vol. 63, no. 10, pp. 6557–6567, Oct. 2016.

[22] Y. Zhang, Z. Yan, Z. Liang, S. Li, and C. C. Mi, "A high-power wireless charging system using LCL-N topology to achieve a compact and low-cost receiver," *IEEE Trans. Power Electron.*, vol. 35, no. 1, pp. 131–137, Jan. 2020.

[23] H. Hao, G. A. Covic, and J. T. Boys, "An approximate dynamic model of LCL-*T*-based inductive power transfer power supplies," *IEEE Trans. Power Electron.*, vol. 29, no. 10, pp. 5554–5567, Oct. 2014.

[24] R. Mai, Y. Chen, Y. Zhang, N. Yang, G. Cao, and Z. He, "Optimization of the passive components for an S-LCC topology-based WPT system for charging massive electric bicycles," *IEEE Trans. Ind. Electron.*, vol. 65, no. 7, pp. 5497–5508, Jul. 2018.

[25] H. Feng, T. Cai, S. Duan, J. Zhao, X. Zhang, and C. Chen, "An LCC-compensated resonant converter optimized for robust reaction to large coupling variation in dynamic wireless power transfer," *IEEE Trans. Ind. Electron.*, vol. 63, no. 10, pp. 6591–6601, Oct. 2016.

[26] X. Dai, Y. Huang, and Y. Li, "Topology comparison and selection of wireless power transfer system and parameter optimization for high voltage gain," in *Proc. IEEE PELS Workshop Emerg. Technol., Wireless Power Transf. (WoW)*, Chongqing, China, May 2017, pp. 1–5.

[27] T. Kan, T.-D. Nguyen, J. C. White, R. K. Malhan, and C. C. Mi, "A new integration method for an electric vehicle wireless charging system using LCC compensation topology: Analysis and design," *IEEE Trans. Power Electron.*, vol. 32, no. 2, pp. 1638–1650, Feb. 2017.

[28] W. Li, H. Zhao, J. Deng, S. Li, and C. C. Mi, "Comparison study on SS and double-sided LCC compensation topologies for EV/PHEV wireless chargers," *IEEE Trans. Veh. Technol.*, vol. 65, no. 6, pp. 4429–4439, Jun. 2016.

[29] S. Li, W. Li, J. Deng, T. D. Nguyen, and C. C. Mi, "A double-sided LCC compensation network and its tuning method for wireless power transfer," *IEEE Trans. Veh. Technol.*, vol. 64, no. 6, pp. 2261–2273, Jun. 2015.

[30] C. Liao and C. A. o. S. Institute of Electrical Engineering, "Design of LCC impedance matching circuit for wireless power transfer system under rectifier load," *CPSS Trans. Power Electron. Appl.*, vol. 2, no. 3, pp. 237–245, Sep. 2017.

[31] V.-B. Vu, D.-H. Tran, and W. Choi, "Implementation of the constant current and constant voltage charge of inductive power transfer systems with the double-sided LCC compensation topology for electric vehicle battery charge applications," *IEEE Trans. Power Electron.*, vol. 33, no. 9, pp. 7398–7410, Sep. 2018.

[32] S. Lu, X. Deng, W. Shu, X. Wei, and S. Li, "A new ZVS tuning method for double-sided LCC compensated wireless power transfer system," *Energies*, vol. 11, no. 2, p. 307, Feb. 2018.

[33] J. L. Villa, J. Sallan, J. F. Sanz Osorio, and A. Llombart, "High-misalignment tolerant compensation topology for ICPT systems," *IEEE Trans. Ind. Electron.*, vol. 59, no. 2, pp. 945–951, Feb. 2012.

[34] J. Hou, Q. Chen, S.-C. Wong, C. K. Tse, and X. Ruan, "Analysis and control of series/series-parallel compensated resonant converter for contactless power transfer," *IEEE J. Emerg. Sel. Topics Power Electron.*, vol. 3, no. 1, pp. 124–136, Mar. 2015.

[35] H. Feng, T. Cai, S. Duan, X. Zhang, H. Hu, and J. Niu, "A dual-side-detuned series–series compensated resonant converter for wide charging region in a wireless power transfer system," *IEEE Trans. Ind. Electron.*, vol. 65, no. 3, pp. 2177–2188, Mar. 2018.

[36] R. Mai, Z. Yan, Y. Chen, S. Liu, and Z. He, "A hybrid transmitter-based efficiency improvement controller with full-bridge dual resonant tank for misalignment condition," *IEEE Trans. Power Electron.*, vol. 35, no. 1, pp. 1124–1135, Jan. 2020.

[37] N. A. Keeling, G. A. Covic, and J. T. Boys, "A unity-power-factor IPT pickup for high-power applications," *IEEE Trans. Ind. Electron.*, vol. 57, no. 2, pp. 744–751, Feb. 2010.

JUNFENG YANG (Member, IEEE) received the B.S. degree in electrical engineering from Beijing Jiaotong University, Beijing, China, in 2012, where he is currently pursuing the Ph.D. degree in electrical engineering. His research interests include power electronics and wireless power transfer.

XIAODONG ZHANG received the M.Sc. degree in communication and information system from Tianjin University, Tianjin, China, in 1991, and the Ph.D. degree in electromagnetic compatibility from Beijing Jiaotong University, Beijing, China, in 2012. Since 1993, he has been with the School of Electrical Engineering, Beijing Jiaotong University. His research interests include electromagnetic compatibility, power electronics, and wireless power transfer.

KAIJIAN ZHANG was born in Beijing, China, in 1996. He received the B.S. degree in mechanical and electronic engineering from Beijing Jiaotong University, Beijing, China, in 2018. He is currently pursuing the M.S. degree with the School of Computer Science and Engineering, University of New South Wales, Australia. His research interests include power electronics, design and optimization of data structure, and database systems.

XIAOYAN CUI was born in 1958. She has been a Professor with the School of Automation, Beijing University of Posts and Telecommunications. Her research interests include wireless sensor networks and energy management.

CHAOQUN JIAO received the M.Sc. and Ph.D. degrees in electrical theory and new technology from North China Electric Power University, Hebei, China, in 2003 and 2006, respectively. Since 2006, he has been with the School of Electrical Engineering, Beijing Jiaotong University. His research interests include electrical theory and new technology, ultra high-voltage technology, and wireless power transfer.

XU YANG (Student Member, IEEE) received the B.Sc. degree from the School of Electrical and Electronic Engineering, Changchun University of Technology, Jilin, China, in 2010, and the M.Sc. degree in electrical engineering from Henan Polytechnic University, Henan, China, in 2013. He is currently pursuing the Ph.D. degree with the School of Electrical Engineering, Beijing Jiaotong University, Beijing, China. His research interests include wireless power transfer applications and power electronic converters.